Biomedical Optics EXPRESS

Near-infrared light photoacoustic ophthalmoscopy

Tan Liu,[1] Qing Wei,[1] Wei Song,[1,4] Janice M. Burke,[2] Shuliang Jiao,[3] and Hao F. Zhang[1,5,*]

[1]*Department of Biomedical Engineering, Northwestern University, Evanston, IL 60208, USA*
[2]*Department of Ophthalmology, The Medical College of Wisconsin, 925 N. 87th Street, Milwaukee, WI 53226, USA*
[3]*Department of Ophthalmology, University of Southern California, Los Angeles, CA 90033, USA*
[4]*Department of Physics, Harbin Institute of Technology, 92 West Da-Zhi Street Nangang District, Harbin, Heilongjiang 150080, China*
[5]*Department of Ophthalmology, Northwestern University, Chicago, IL 60611, USA*
**hfzhang@northwestern.edu*

Abstract: We achieved photoacoustic ophthalmoscopy (PAOM) imaging of the retina with near-infrared (NIR) light illumination. A PAOM imaging system with dual-wavelength illumination at 1064 nm and 532 nm was built. We compared *in vivo* imaging results of both albino and pigmented rat eyes at the two wavelengths. The results show that the bulk optical absorption of the retinal pigment epithelium (RPE) is only slightly higher than that of the retinal vessels at 532 nm while it becomes more than an order of magnitude higher than that of the retinal vessels at 1064 nm. These studies suggest that although visible light illumination is suitable for imaging both the retinal vessels and the RPE, NIR light illumination, being more comfortable to the eye, is better suited for RPE melanin related investigations and diagnoses.

OCIS codes: (110.5120) Photoacoustic imaging; (170.4470) Ophthalmology.

References and Links

1. S. Jiao, M. Jiang, J. Hu, A. Fawzi, Q. Zhou, K. K. Shung, C. A. Puliafito, and H. F. Zhang, "Photoacoustic ophthalmoscopy for *in vivo* retinal imaging," Opt. Express **18**(4), 3967–3972 (2010).
2. Q. Wei, T. Liu, S. Jiao, and H. F. Zhang, "Image chorioretinal vasculature in albino rats using photoacoustic ophthalmoscopy," J. Mod. Opt. **58**(21), 1997–2001 (2011).
3. H. F. Zhang, K. Maslov, and L. V. Wang, "*In vivo* imaging of subcutaneous structures using functional photoacoustic microscopy," Nat. Protoc. **2**(4), 797–804 (2007).
4. H. F. Zhang, K. Maslov, G. Stoica, and L. V. Wang, "Functional photoacoustic microscopy for high-resolution and noninvasive *in vivo* imaging," Nat. Biotechnol. **24**(7), 848–851 (2006).
5. T. Liu, Q. Wei, J. Wang, S. Jiao, and H. F. Zhang, "Combined photoacoustic microscopy and optical coherence tomography can measure metabolic rate of oxygen," Biomed. Opt. Express **2**(5), 1359–1365 (2011).
6. J. Yao, K. I. Maslov, Y. Zhang, Y. Xia, and L. V. Wang, "Label-free oxygen-metabolic photoacoustic microscopy *in vivo*," J. Biomed. Opt. **16**(7), 076003 (2011).
7. X. Zhang, H. F. Zhang, C. A. Puliafito, and S. Jiao, "Simultaneous *in vivo* imaging of melanin and lipofuscin in the retina with photoacoustic ophthalmoscopy and autofluorescence imaging," J. Biomed. Opt. **16**(8), 080504 (2011).
8. W. Song, Q. Wei, T. Liu, D. Kuai, J. M. Burke, S. Jiao, and H. F. Zhang, "Integrating photoacoustic ophthalmoscopy with scanning laser ophthalmoscopy, optical coherence tomography, and fluorescein angiography for a multimodal retinal imaging platform," J. Biomed. Opt. (to be published).
9. American National Standards Institute (ANSI), "American national standard for the safe use of lasers," Standard Z136.1–2007 (Laser Institute of America, Orlando, FL, 2007).
10. P. E. Stanga, J. I. Lim, and P. Hamilton, "Indocyanine green angiography in chorioretinal diseases: indications and interpretation: an evidence-based update," Ophthalmology **110**(1), 15–21, quiz 22–23 (2003).
11. S. Schmitz-Valckenberg, J. S. Steinberg, M. Fleckenstein, S. Visvalingam, C. K. Brinkmann, and F. G. Holz, "Combined confocal scanning laser ophthalmoscopy and spectral-domain optical coherence tomography imaging of reticular drusen associated with age-related macular degeneration," Ophthalmology **117**(6), 1169–1176 (2010).

#163768 - $15.00 USD
Received 27 Feb 2012; accepted 12 Mar 2012; published 27 Mar 2012

12. M. Han, G. Giese, S. Schmitz-Valckenberg, A. Bindewald-Wittich, F. G. Holz, J. Yu, J. F. Bille, and M. H. Niemz, "Age-related structural abnormalities in the human retina-choroid complex revealed by two-photon excited autofluorescence imaging," J. Biomed. Opt. **12**(2), 024012 (2007).
13. J. J. Hunter, B. Masella, A. Dubra, R. Sharma, L. Yin, W. H. Merigan, G. Palczewska, K. Palczewski, and D. R. Williams, "Images of photoreceptors in living primate eyes using adaptive optics two-photon ophthalmoscopy," Biomed. Opt. Express **2**(1), 139–148 (2011).
14. V. M. Kodach, J. Kalkman, D. J. Faber, and T. G. van Leeuwen, "Quantitative comparison of the OCT imaging depth at 1300 nm and 1600 nm," Biomed. Opt. Express **1**(1), 176–185 (2010).
15. R. K. Wang and L. An, "Multifunctional imaging of human retina and choroid with 1050-nm spectral domain optical coherence tomography at 92-kHz line scan rate," J. Biomed. Opt. **16**(5), 050503 (2011).
16. S. Jiao, R. Knighton, X. Huang, G. Gregori, and C. Puliafito, "Simultaneous acquisition of sectional and fundus ophthalmic images with spectral-domain optical coherence tomography," Opt. Express **13**(2), 444–452 (2005).
17. S. Hu, B. Rao, K. Maslov, and L. V. Wang, "Label-free photoacoustic ophthalmic angiography," Opt. Lett. **35**(1), 1–3 (2010).
18. A. Hughes and H. Wässle, "An estimate of image quality in the rat eye," Invest. Ophthalmol. Vis. Sci. **18**(8), 878–881 (1979).
19. M. Hammer, A. Roggan, D. Schweitzer, and G. Müller, "Optical properties of ocular fundus tissues--an *in vitro* study using the double-integrating-sphere technique and inverse Monte Carlo simulation," Phys. Med. Biol. **40**(6), 963–978 (1995).
20. M. Kinnunen and R. Myllylä, "Effect of glucose on photoacoustic signals at the wavelengths of 1064 and 532-nm in pig blood and Intralipid," J. Phys. D Appl. Phys. **38**(15), 2654–2661 (2005).
21. S. L. Jacques, "Melanosome absorption coefficient," http://omlc.ogi.edu/spectra/melanin/mua.html.
22. L. N. Thibos, A. Bradley, D. L. Still, X. Zhang, and P. A. Howarth, "Theory and measurement of ocular chromatic aberration," Vision Res. **30**(1), 33–49 (1990).
23. K. Maslov, H. F. Zhang, and L. V. Wang, "Effects of wavelength-dependent fluence attenuation on the noninvasive photoacoustic imaging of hemoglobin oxygen saturation in subcutaneous vasculature *in vivo*," Inverse Probl. **23**(6), S113–S122 (2007).
24. C. N. Keilhauer and F. C. Delori, "Near-infrared autofluorescence imaging of the fundus: visualization of ocular melanin," Invest. Ophthalmol. Vis. Sci. **47**(8), 3556–3564 (2006).
25. U. Kellner, S. Kellner, and S. Weinitz, "Fundus autofluorescence (488 NM) and near-infrared autofluorescence (787 NM) visualize different retinal pigment epithelium alterations in patients with age-related macular degeneration," Retina **30**(1), 6–15 (2010).
26. X. Zhang, H. F. Zhang, and S. Jiao, "Optical coherence photoacoustic microscopy: accomplishing optical coherence tomography and photoacoustic microscopy with a single light source," J. Biomed. Opt. **17**(3), 030502 (2012).
27. J. W. You, T. C. Chen, M. Mujat, B. H. Park, and J. F. de Boer, "Pulsed illumination spectral-domain optical coherence tomography for human retinal imaging," Opt. Express **14**(15), 6739–6748 (2006).
28. S. Moon and D. Y. Kim, "Ultra-high-speed optical coherence tomography with a stretched pulse supercontinuum source," Opt. Express **14**(24), 11575–11584 (2006).
29. Q. Zhou, S. Lau, D. Wu, and K. K. Shung, "Piezoelectric films for high frequency ultrasonic transducers in biomedical applications," Prog. Mater. Sci. **56**(2), 139–174 (2011).
30. T. Ling, S. L. Chen, and L. J. Guo, "Fabrication and characterization of high Q polymer micro-ring resonator and its application as a sensitive ultrasonic detector," Opt. Express **19**(2), 861–869 (2011).

1. Introduction

Photoacoustic ophthalmoscopy (PAOM) [1] is a newly developed photoacoustic (PA) imaging technology that is complementary to the existing ophthalmic imaging technologies by providing optical absorption imaging contrast. The benefits of PAOM arise from its intrinsic absorption contrast which enables PAOM to visualize strongly optically absorbing tissue (e.g. blood vessels in the retina and choroid, and the retinal pigmented epithelium) with a high signal to noise ratio [1,2]; in the meantime, imaging optical absorption properties at multiple wavelengths can extract important hemodynamic information such as oxygenation saturation [3–6], which can be potentially applied to sensing retinal hemodynamic functions. Previously, we demonstrated the PAOM imaging of retinal microvascular network, the retinal pigmented epithelium (RPE), and choroid capillary network [1,2]. We also showed the capability of PAOM to provide complementary *in vivo* anatomical information by integrating it with autofluorescence imaging [7], scanning laser ophthalmoscopy, spectral-domain optical coherence tomography (SD-OCT) and fluorescein angiography [8].

The existing PAOM uses visible light for imaging the retina, which has two disadvantages compared to infrared (NIR) light. First, visible light illumination is uncomfortable to the eye.

#163768 - $15.00 USD Received 27 Feb 2012; accepted 12 Mar 2012; published 27 Mar 2012

Second, according to ANSI safety standard [9], visible light has lower ocular damage threshold than NIR light, i.e. the NIR light is much safer than the visible light for ocular imaging. As a result, using NIR light can be more acceptable by patients and developing a NIR light PAOM can be very beneficial.

NIR light has been widely used in many well-established ophthalmic imaging technologies. For example, indocyanine green angiography (ICGA) using 810-nm illumination light to deliver optical energy through the melanin-rich RPE [10], confocal scanning laser ophthalmoscopy using 830-nm light source instead of traditional visible light to visualize drusen [11], two-photon autofluorescence microscopy employing NIR light to image retina layer and choroid layer [12] and photoreceptors *in vivo* [13]. Existing SD-OCT primarily uses 830-nm light for clinical imaging and researchers are also using optical wavelengths longer than 1 μm to image the deeper choroid [14,15].

In this paper, we report our latest work on NIR light PAOM. We developed a dual-wavelength illumination PAOM that employs 1064-nm and 532-nm optical illuminations and applied it to image both albino and pigmented rat eyes. A discussion on ocular laser safety within NIR spectral range is also given.

2. Methods and materials

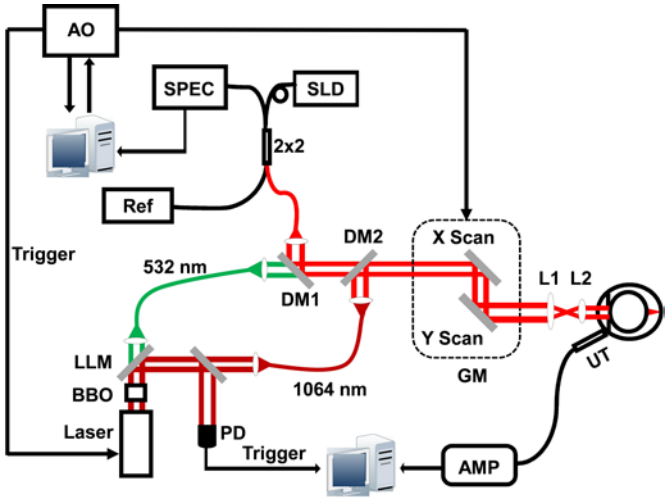

Fig. 1. Schematic of the dual-wavelength PAOM guided by SD-OCT. PD: photodiode; DM: dichroic mirror; GM: 2D galvanometer mirrors; AMP: amplifier; UT: ultrasonic transducer; AO: analogous output board; SLD: super-luminescent laser diode; Ref: OCT reference arm; 2 × 2: 50:50 fiber coupler; L1: relay lens; L2: objective lens; LLM: laser line mirror.

2.1. System setup

A schematic diagram of the dual-wavelength PAOM is shown in Fig. 1. We integrated a SD-OCT with the dual- wavelength PAOM for optical alignment purposes [1]. We used a Nd:YAG laser (SPOT-10-100, Elforlight Ltd, UK; output wavelength: 1064 nm; maximum pulse energy: 20 μJ; pulse duration: 2 ns; maximum pulse repetition rate: 30 kHz) as the irradiation source for PAOM. A beta-barium-borate (BBO) crystal (CasTech, San Jose, CA) was used to achieve frequency doubling of the output 1064-nm laser light. Then the 1064-nm and 532-nm light were separated by a laser line mirror (> 99.5% reflection at 1064-nm and > 95% transmission at 532-nm at 45 degrees) and were coupled into two single-mode optical fibers. The SD-OCT used a broadband super-luminescent diode (SLD) as the light source (IPSDD0804, InPhenix; center wavelength λ_0: 840 nm; 3-dB bandwidth $\Delta\lambda$: 50 nm). The 532-nm light coming out of the fiber was combined with the SD-OCT probing light by a dichroic mirror (DM1 in Fig. 1, NT43-955, Edmund Optics) and was further combined with the 1064-

#163768 - $15.00 USD Received 27 Feb 2012; accepted 12 Mar 2012; published 27 Mar 2012

nm light by a second dichroic mirror (DM2 in Fig. 1, DMSP1000, Thorlabs). Then the combined beams were scanned by an x–y galvanometer (QS-7, Nutfield Technology) and delivered to the posterior segment of the eye after passing through a relay lens L1 (f = 76.2 mm, NT49-794, Edmund Optics) and an objective lens L2 (f = 14 mm, NT49-658, Edmund Optics).

For PAOM detection, we used a custom-built unfocused needle ultrasonic transducer (central frequency 35 MHz; bandwidth: 50%; active element size: 1×1 mm^2). The ultrasonic transducer was placed in gentle contact with the eyelid coupled by ultrasound gel. The detected PAOM signals were amplified by 65 dB before being digitized and stored. For SD-OCT detection, we used a home-built spectrometer as detailed previously [16].

The PAOM and SD-OCT acquisition were synchronized. An analogue output board (PCI-6731, National Instruments) triggered both the PAOM laser firing and the image acquisition board for the CCD camera in the SD-OCT spectrometer and controlled the galvanometer. To avoid jittering associated with the illumination lasers, the PAOM data acquisition board (CS 14200, Gage Applied) was triggered by a photodiode (PD in Fig. 1), which also sampled the laser output energy.

In the dual-wavelength system, the PAOM and the SD-OCT worked at a 20 kHz A-line rate. To acquire a full-field fundus image, the scan angle was 26°, which covered an area of approximately 2.8×2.8 mm^2 on a rat retina. The raster scanning includes 256×256 pixels. During data acquisition, only one PAOM illumination wavelength (either 532-nm or 1064-nm) was used at a time. Because the 532-nm and 1064-nm light were well aligned, the PAOM images acquired at these two wavelengths were intrinsically registered.

In *in vivo* retinal imaging, the PAOM and SD-OCT have a comparable lateral resolution of ~20 μm. The axial resolution of PAOM is 23 μm, which is determined by the ultrasonic bandwidth, and the axial resolution of the SD-OCT is 6 μm, which is determined by the bandwidth of the light source [1].

2.2. Ocular laser safety

The laser pulse energy used in the PAOM system strictly follows the ANSI ocular laser safety standard [9]. In our experiments, the mean power of the SD-OCT probing light was 0.8 mW and laser pulse energy of PAOM (at 532-nm illumination) was 40 nJ, all of which are considered safe [1,9,17]. Here we further provide a detailed derivation of the maximum permissible exposure (MPE) when PAOM works at the 1064-nm illumination.

The ocular MPE of incident laser depends on the optical wavelength, pulse duration, exposure duration, and exposure aperture. Since no signal averaging was used in PAOM, each scanning location on the retina was exposed to only a single laser pulse. In rodent eye imaging, the laser focusing spot on the retina is around 20 μm. PAOM illuminating pulses will not overlap with each beyond a scanning distance of 20 μm, which corresponds to an angular subtense $\alpha = 3.33$ mrad when considering that the axial length of a rat eye chamber is 6 mm. As a result, the PAOM illumination source is an extended light source [9]. And we have $\alpha_{min} < \alpha < \alpha_{max}$, where α_{min} (1.5 mrad) and α_{max} (100 mrad) are the minimal and maximal subtense angles, respectively, for wavelength between 0.4 and 1.4 μm defined in Ref. [9]. According to Table 6 of Ref. [9], the correction factors C_C and C_E are 1.0 and $\alpha/\alpha_{min} = 2.22$, respectively. To identify the minimal MPE, all the three rules described in the section 8.2.3 in Ref. [9] need to be taken into consideration.

Rule 1. Single pulse limit (MPE_{SP}). This rule requires that "the exposure from any single pulse in a train of pulses shall not exceed the MPE for a single pulse of that pulse duration" [9]. According to the ANSI safety standard, when the optical wavelength is between 1.05 μm and 1.40 μm and pulse duration is between 10^{-9} s and 50×10^{-6} s, the $MPE_{SP} = 5.0 C_C C_E \times 10^{-6}$ J/cm^2 $= 1.11 \times 10^{-5}$ J/cm^2.

Rule 2. Average power limit for thermal hazard (MPE_{GROUP}). It means that "the total radiant exposure of all pulses within any part of the train shall not exceed the MPE for the

#163768 - $15.00 USD Received 27 Feb 2012; accepted 12 Mar 2012; published 27 Mar 2012

duration of that part" [9]. The photochemical hazard limit is not applied into our situation since the illumination wavelength is in the NIR range. Within the 3.33 mrad, we consider that we will have maximally n = 10 points in the over-sampling mode with pulses overlapping with each other. At a PRF of 20 kHz, the time span for this group of over-sampling will take 0.5 ms. As a result, we have $MPE_{GROUP} = 9.0C_CC_Et_{GROUP}^{0.75} \times 10^{-3} = 6.68 \times 10^{-5}$ J/cm^{-2}, and the average pulse power is $MPE_{GROUP}/n = 6.68 \times 10^{-6}$ J/cm^{-2}.

Rule 3. Multiple pulse limit for thermal hazard (MPE_{MP}). The MPE_{MP} is limited by MPE_{SP} multiple by a correction factor $C_P = n^{-0.25}$. In our case, we have $C_p = 0.562$ and $MPE_{MP} = 6.24 \times 10^{-6}$ J/cm^{-2}.

Based on the above calculations, Rule 3 dominates. By using equation $E_{pulse}/A = MPE$, where $MPE = MPE_{MP}$ and A is the rat pupil size, the energy of each pulse is given by $E_{pulse} = 6.24 \times 10^{-6} \times 0.09$ J = 562 nJ, where a dilated rat's pupil has an diameter of 3 mm [18]. In our experiment, the pulse energy at 1064 nm illumination was around 450 nJ.

2.3. Animal preparations

We imaged wild-type Sprague Dawley and Long Evans rats (300-600 g, Charles Rivers Laboratories). The rats were anesthetized and kept motionless by a mixture of 1.5% isoñurane and oxygen at a flow rate of 1.5 liter/minute. During imaging, the animals were placed in a homemade animal holder. We applied 0.5% Tetracaine Hydrochloride ophthalmic solution to the rat eyes for local anesthesia and applied 1% Tropicamide ophthalmic solution to dilate the pupil. Commercial artificial tears were applied to the rat eyes every other minute to prevent cornea dehydration. The rats were removed from the imaging setup immediately after experiments and they recovered without noticeable retinal damages in the follow-up examinations using SD-OCT.

All experiments were performed in compliance with the ARVO Statement for the Use of Animals in Ophthalmic and Vision Research, as well as the laboratory animal protocol approved by the Animal Care and Use Committee of Northwestern University.

3. Results and discussions

3.1. Comparison between visible and NIR light PAOM results

An advantage of PAOM is its capability to image various optical absorbing substances by tuning the illuminating optical wavelength [3]. According to the literature data, from 532-nm to 1064-nm the optical absorption coefficient of whole blood drops more than 40-fold, but the optical absorption coefficient of melanin (not RPE) drops 4-10-fold [19-21]. Therefore, when illuminated at 1064-nm the RPE may generate stronger PA signals than hemoglobin and could be imaged with higher contrast with respect to the vascular network comparing to the images acquired at 532 nm.

Figure 2 compares the visible and NIR light PAOM images. Figure 2(a) and Fig. 2(b) are from a pigmented rat eye. Figure 2(a) is acquired at 532 nm, where the molar extinction coefficients of both hemoglobin and melanin are strong. When illuminated with NIR light (Fig. 2(b)), the overall PA signal amplitude decreased due to weaker optical absorption. However, more vascular anatomic features than those in Fig. 2(a) are observed. As pointed out by the group 1 arrows, these three minor vessels were not well resolved in Fig. 2(a); however, they became much better visualized in Fig. 2(b). As pointed out by the group 2 arrows, these vessels are well-resolved in the NIR PAOM image but do not show up in Fig. 2(a). Moreover, we could see that all the vessels being pointed out by both arrow groups are branches of the major retinal vessels. Note that all the vessels pointed out in Fig. 2(b) are "shadows" on the RPE.

Several reasons could lead to the difference between PAOM images acquired at the two wavelengths. We hypothesize that these minor vessel branches are deeper into the retinal and the imaged difference is caused by the axial chromatic aberration [22] of the imaging optics and the eye itself because longer optical wavelength focuses deeper.

#163768 - $15.00 USD Received 27 Feb 2012; accepted 12 Mar 2012; published 27 Mar 2012

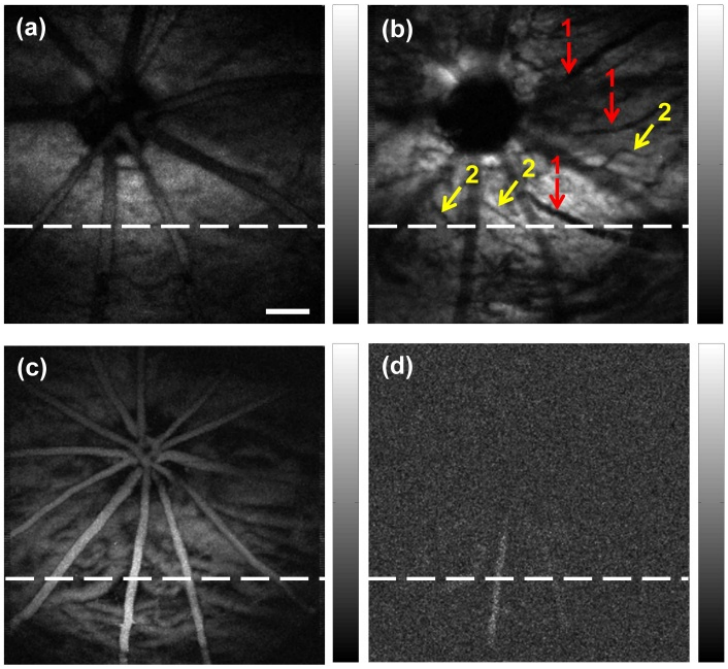

Fig. 2. Comparison of visible and NIR light PAOM images. (a) and (b) are *in vivo* images acquired at 532 nm and 1064 nm in a pigmented rat, respectively; (c) and (d) are *in vivo* images acquired at 532 nm and 1064 nm in an albino rat, respectively. Bar: 250 μm.

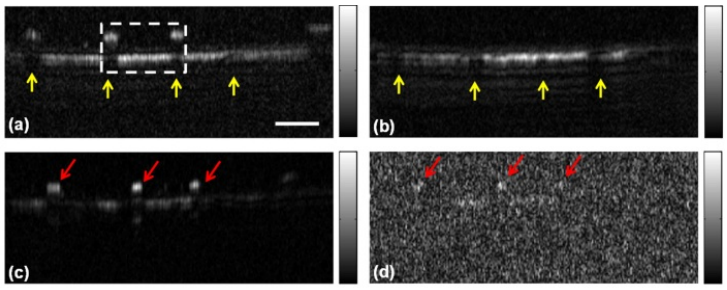

Fig. 3. Comparison of visible and NIR PAOM B-scan images. (a) and (b) are images acquired at 532-nm and 1064-nm in a pigmented rat, respectively; (c) and (d) are images acquired at 532-nm and 1064-nm in an albino rat, respectively. Bar: 250 μm.

Figure 2(c) and Fig. 2(d) are visible and NIR light PAOM images from an albino eye. Both retinal and choroidal vascular networks are visualized in the visible light PAOM image due to the lack of RPE melanin. Because of the much reduced blood absorption, almost no vascular network can be imaged using NIR light (Fig. 2(d)).

Figure 3 compares the visible and NIR light PAOM B-scan images at positions marked in Fig. 2. We could observe that due to stronger melanin optical absorption than the much reduced hemoglobin optical absorption at 1064 nm, retinal vessels that were clearly imaged in Fig. 3(a) disappeared in Fig. 3(b); however, the shadows on the RPE created by retinal vessels are identical between Fig. 3(a) and Fig. 3(b) as highlighted. Similar effects can be observed in the albino rat eye, where strong PA signals are generated from retinal and choroidal vascular network in the visible light image (Fig. 3(c)) yet only weak PA signals were detected in the NIR light image (Fig. 3(d)), which are around the same amplitude level of random noise, as pointed out by the red arrows.

#163768 - $15.00 USD
Received 27 Feb 2012; accepted 12 Mar 2012; published 27 Mar 2012

A more quantitative comparison of the PA amplitudes from retinal vessels and the RPE/choroid complex when illuminated with 532-nm and 1064-nm light are given in Fig. 4. These typical values were extracted from the region highlighted by the dashed-box in Fig. 3(a). When illuminated with 532-nm light, PA signal amplitudes of both retinal vessels and the RPE/choroid complex are comparable and are much stronger than the values from 1064-nm light illumination. However, in the NIR image, RPE generates much stronger PA signal than retinal vessels, which makes the PAOM imaging more melanin specific.

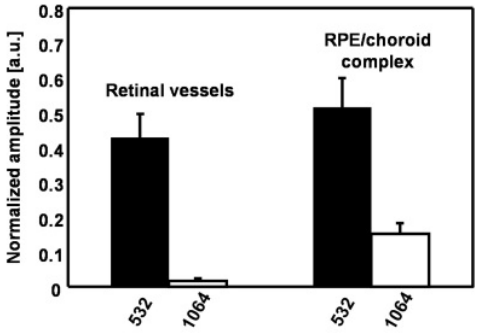

Fig. 4. Comparison of PA amplitudes from retinal vessels and RPE/choroid complex when illuminated by visible and NIR light in a pigmented rat eye.

We believe that NIR light PAOM can better visualize melanin in the RPE while minimizing the influence coming from blood vessel shadowing. Previous studies [23] have showed that the PA signal amplitude depends on the local light intensity and the local optical absorbing coefficient within each voxel. Since the attenuation of the PAOM illumination by the anterior segment and the vitreous within the NIR optical spectrum range is minimal, the projection images shown in Fig. 2(b) reflect the spatial distribution of melanin content in the RPE/choroid. Because of the decreased optical absorption of melanin, NIR light can penetrate through the RPE and induce PA signals from choroidal melanin. Due to the currently limited axial resolution of PAOM (~23 μm), contributions from the RPE melanin and the choroidal melanin are hard to be separated, which is similar to the NIR autofluorescence imaging [24,25].

3.2. NIR light PAOM has potential to share illumination source with other modalities

In our current work, we used two independent light sources for PAOM and SD-OCT. Having the feasibility of NIR light PAOM demonstrated, we can potentially use a wideband NIR light source for both PAOM and SD-OCT. Previously we demonstrated that SD-OCT and photoacoustic microscopy can in fact share a wideband visible light source for dual-modality imaging [26]. The drawback of visible-light SD-OCT is the limited penetration depth due to stronger optical absorption and scattering than NIR light in tissue. If an appropriate wideband NIR light can be identified, NIR light PAOM can be achieved with high-spatial resolution, deep-penetrating SD-OCT for more comprehensive studies of the RPE/choroid. Such a wideband NIR can potentially be generated by super-continuum from a photonic crystal fiber pumped by femtosecond laser pulses [27,28].

3.3. Methods to improve the axial resolution of PAOM

The axial resolution of PAOM is primarily limited by the bandwidth of the ultrasound detectors [29]. To image adjacent tissue anatomies, such as RPE and choroid capillaries, an axial resolution higher than 10 μm is needed. Novel ultrasound detectors, such as optical micro ring resonator based ultrasound sensor [30], can be used to improve the axial resolution PAOM. Because of the extremely wide detection bandwidth of the optical micro-ring resonator [30], we expect that the axial resolution can be significantly improved.

#163768 - $15.00 USD Received 27 Feb 2012; accepted 12 Mar 2012; published 27 Mar 2012

4. Conclusion

In conclusion, we developed a dual-wavelength (532 nm and 1064 nm) PAOM and further integrated it with SD-OCT to image rat eyes. We demonstrated the feasibility of NIR-light PAOM *in vivo*. Due to the much reduced optical absorption coefficient of hemoglobin within the NIR spectral range, the NIR light PAOM is not suitable for imaging the retinal and choroidal blood vessels with laser pulse energies below the safety limit. However, in pigmented rats the NIR light PAOM successfully imaged the RPE/choroidal melanin with good SNR. We believe that NIR light is better suited for future clinical applications of PAOM for melanin-related imaging because that NIR excitation is safer and more comfortable to the patient eyes. NIR light PAOM also opens up new possibilities for PAOM to be integrated with SD-OCT by sharing a single wideband NIR light source.

Acknowledgments

This work is supported in part by the National Institutes of Health (1RC4EY021357 and 1R01EY019951) and the National Science Foundation (CAREER CBET-1055379).

#163768 - $15.00 USD Received 27 Feb 2012; accepted 12 Mar 2012; published 27 Mar 2012